Can oceanic submesoscale processes be observed with satellite altimetry?

Cédric P. Chavanne[1] and Patrice Klein[2]

Received 9 August 2010; revised 26 September 2010; accepted 30 September 2010; published 18 November 2010.

[1] High-resolution (2 km and hourly) observations of surface currents from High-Frequency Radars are analyzed in terms of sea level anomalies (SLA) and compared with data from two satellite altimeter ground tracks. Purpose is to investigate whether ocean submesoscale processes can be observed with satellite altimetry. Our results highlight two major problems that must be overcome before being able to resolve submesoscale processes with altimetry: (i) signal contamination from high-frequency motions and in particular from incoherent internal tides (near-inertial oscillations have no effect on SLA), and (ii) measurement noise which prevents the computation of accurate cross-track currents on scales $\mathcal{O}$ (10 km). The latter may be overcome by future satellite altimeter missions, but the former will require taking into account the effect of mesoscale variability on internal tide propagation in regions where internal tides are significant. **Citation:** Chavanne, C. P., and P. Klein (2010), Can oceanic submesoscale processes be observed with satellite altimetry?, *Geophys. Res. Lett.*, *37*, L22602, doi:10.1029/2010GL045057.

1. Introduction

[2] Satellite altimetry has revolutionized our ability to observe ocean mesoscale $\mathcal{O}$ (100 km) processes, which account for most of the sub-inertial horizontal kinetic energy [*Chelton et al.*, 2007]. Submesoscale $\mathcal{O}$ (10 km) processes on the other hand appear to explain much of the sub-inertial vertical kinetic energy in the upper ocean [*Klein et al.*, 2008; *Capet et al.*, 2008]. The latter play an important part in the vertical exchange of properties, enhancing in particular nutrient supply to the euphotic layer. Submesoscale processes are not resolved by gridded altimeter-derived Sea Level Anomalies (SLAs), owing to the large spacing between satellite ground tracks [*Ducet et al.*, 2000]. Along-track SLAs are available at horizontal resolutions of 6–7 km, sufficient in theory to resolve the upper range of submesoscale processes. But observation of submesocale processes using satellite SLA data requires first to question the contribution of higher frequency motions to SLA since these motions may be energetic at $\mathcal{O}$ (10 km) horizontal scales [*Klein et al.*, 2004; *Chavanne et al.*, 2010d].

[3] We take advantage of high-resolution observations from High-Frequency Radars (HFRs) deployed on the west shore of O'ahu, Hawai'i (providing 2-km resolution hourly surface currents, see *Chavanne et al.* [2010d] for a description of the processing) and the crossing of two satellite altimeter ground tracks, Geosat Follow-On (GFO) track 13 and Jason-1 (JAS) track 223 (providing 6–7 km resolution along-track SLAs), over the HFR observational domain (Figure 1), to understand the relative importance of high-frequency (near-inertial and super-inertial) and low-frequency (sub-inertial) motion contribution to the SLA. The HFR current data were low-pass filtered with a 2-day cut-off period to separate low and high frequency motions (see *Chavanne et al.* [2010a] for details). Satellite SLA data validated, non-filtered, non-subsampled, and corrected for long wavelength errors, were used to retain resolution at the smallest scales observed. A total of 20 altimeter passes are available when the HFRs were measuring surface currents. We focus here on two passes which differ from each other in terms of both the relative importance of low and high frequency motions to SLA (section 2) and the relative importance of coherent and incoherent internal tides to SLA (section 3), that are representative of the range of conditions observed (see auxiliary material).[1]

2. Relative Importance of Low and High Frequency Motions to SLA

[4] A strong submesoscale anticyclone with 15-km radius (Figure 2a) was observed with the HFRs during Fall 2002 (see *Chavanne et al.* [2010a] for a detailed description). The relative vorticity ζ magnitude was close to f, which indicates an $\mathcal{O}(1)$ Rossby number (defined as $Ro = |\zeta|/f$). During Spring 2003 a Rossby wave was observed with again an $\mathcal{O}(1)$ Rossby number and $\mathcal{O}$ (10 km) relative vorticity structures (Figure 3a). Its characteristics are consistent with a Vortex Rossby Wave (VRW), i.e., a Rossby wave propagating through the (radial) gradient of potential vorticity associated with a vortex, here a mesoscale cyclone lying west of O'ahu [*Chavanne et al.*, 2010b]. For both submesoscale structures, amplitudes of high-frequency motions (super-inertial and near-inertial) are weaker than those of subinertial motions (compare in Figures 2c and 2e and Figures 3c and 3e).

[5] GFO-13 crossed over the anticyclone core on 27 October 2002 at 04:54 (UTC), when the anticyclone reached its extremum vorticity [*Chavanne et al.*, 2010a]. SLA from GFO-13 (thin line on Figure 2b) showed a pronounced doming (~6 cm high) centered over the anticyclone core, as expected for anticyclonic vortices in gradient-wind balance in the Northern hemisphere. JAS-223 crossed over the VRW on 26 March 2003 at 06:42 (UTC). SLA from JAS-223 (thin line on Figure 3b) resembled a sine curve with amplitude

[1]School of Environmental Sciences, University of East Anglia, Norwich, UK.
[2]Laboratoire de Physique des Océans, IFREMER-CNRS-UBO-IRD, Plouzane, France.

0094-8276/10/2010GL045057

[1]Auxiliary materials are available in the HTML. doi:10.1029/2010GL045057.

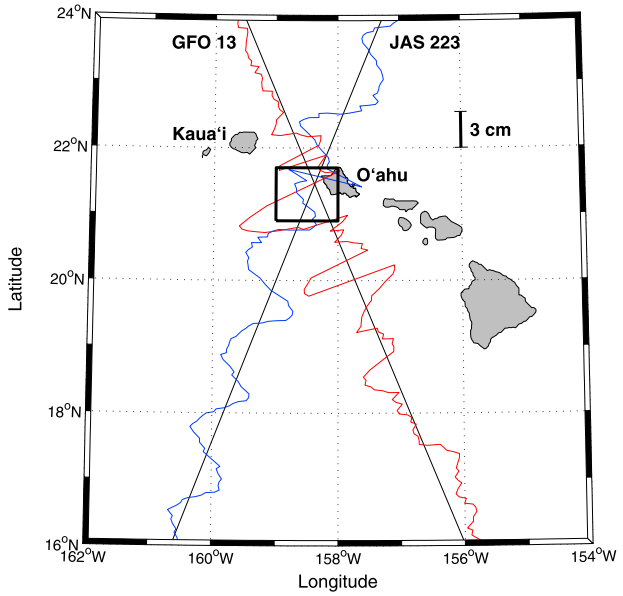

Figure 1. Study area: the main Hawaiian islands are shown in gray, and the area displayed in Figures 2 and 3 is indicated by the black rectangle. SLAs associated with coherent M_2 internal tides are shown along GFO 13 and Jason-1 223 ground tracks (scale given in upper right corner).

~5 cm, as expected for a Rossby wave with approximately unidirectional currents and sinusoidal vorticity structure (Figure 3c) [see also *Chavanne et al.*, 2010c, Figure 4]. These snapshots suggest the possibility to detect similar submesoscale motions over the global ocean with existing altimeters.

[6] We have compared SLAs observed by the altimeters with an estimated SLA, h_{hfr}, obtained by integrating the inviscid primitive equations (PE) momentum balance (neglecting the advective term involving the vertical velocity, which is very small near the surface) for the "instantaneous" (hourly-averaged) HFR currents, (u, v) (Figures 2a and 3a), along the altimeter tracks:

$$h_{hfr}(x) = h_0 - \frac{1}{g}\int_{x_0}^{x}\left(\frac{\partial u}{\partial t} + u\frac{\partial u}{\partial x'} + v\frac{\partial u}{\partial y} - fv\right)dx' \qquad (1)$$

where the current components have been rotated in the along- and across-track directions (x, y), and h_0 is an arbitrary constant specifying the value of SLA at the arbitrary position x_0. Estimated SLAs, h_{hfr}, (thick lines on Figures 2b and 3b) are, for both submesoscale structures, in relatively good agreement with the SLAs observed by the altimeters.

[7] To check whether the h_{hfr} were in gradient-wind balance with the observed surface currents, we computed a new SLA, H_{hfr}, by integrating the inviscid PE momentum balance for the sub-inertial currents, (U, V) (Figures 2c and 3c), along the altimeter tracks:

$$H_{hfr}(x) = H_0 - \frac{1}{g}\int_{x_0}^{x}\left(U\frac{\partial U}{\partial x'} + V\frac{\partial U}{\partial y} - fV\right)dx' \qquad (2)$$

The Eulerian acceleration term, $\partial U/\partial t$ has been neglected since it is much smaller than the Coriolis and advection terms (that have similar magnitude, see also Figure 4b). For the anticyclone, H_{hfr} along GFO track (thick black line on Figure 2d) displays a doming of ~2 cm, i.e., much smaller than that from h_{hfr} or GFO SLA. This highlights a strong contribution of high-frequency motions on h_{hfr} displayed by $h'_{hfr} = h_{hfr} - H_{hfr}$ that yields a doming of ~4 cm (thick black line on Figure 2f). For the VRW on the other hand, H_{hfr} (thick black line on Figure 3d) is closer to h_{hfr}, which indicates a smaller contribution of the high-frequency motions except in the North (thick black line on Figure 3f). We quantify the relative importance of low-frequency and high-frequency contributions to SLA by computing the ratio of their root-mean-square (rms) values along the altimeter tracks: $\alpha_1 = rms(H_{hfr})/rms(h'_{hfr})$. For the GFO pass over the anticyclone, $\alpha_1 = 0.5$, and for the Jason-1 pass over the VRW, $\alpha_1 = 3.2$. These two cases are representative of the 20 passes analyzed since α_1 ranges from 0.1 to 3.2, with 16 passes having $\alpha_1 \leq 1$, indicating a dominant high-frequency contribution for these 16 passes.

3. Contribution of High Frequency Motions to SLA

[8] The high-frequency motions include superinertial motions (mostly tides), and Near-Inertial Oscillations (NIOs)

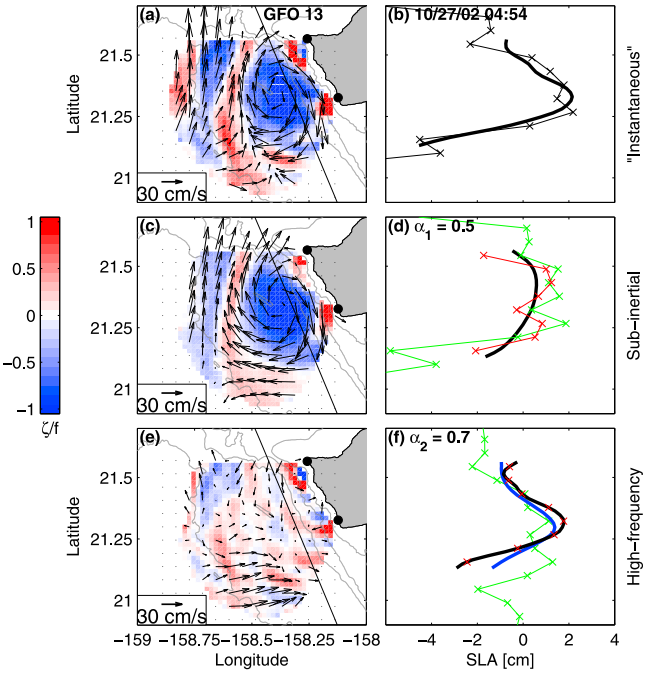

Figure 2. (left) Currents and vorticity (normalized by f) observed from HFRs (black bullets) on 27 October 2002, and (right) SLAs along GFO-13 ground track for (a, b) "instantaneous", (c, d) sub-inertial, and (e, f) high-frequency (near-inertial and super-inertial) flows. In Figure 2b, SLAs computed from HFR currents (thick) and observed from GFO (thin). In Figure 2d, SLAs computed from HFR sub-inertial currents (black) and observed from GFO minus the contribution from coherent internal tides (green) or from HFR high-frequency currents (red). In Figure 2f, SLAs computed from HFR high-frequency currents (black, with red crosses at altimeter grid points) and from coherent tidal currents (blue). Green curve shows GFO SLA associated with coherent internal tides. Bathymetric contours at 500, 1000, 2000 and 4000 m are indicated in gray in the left panels.

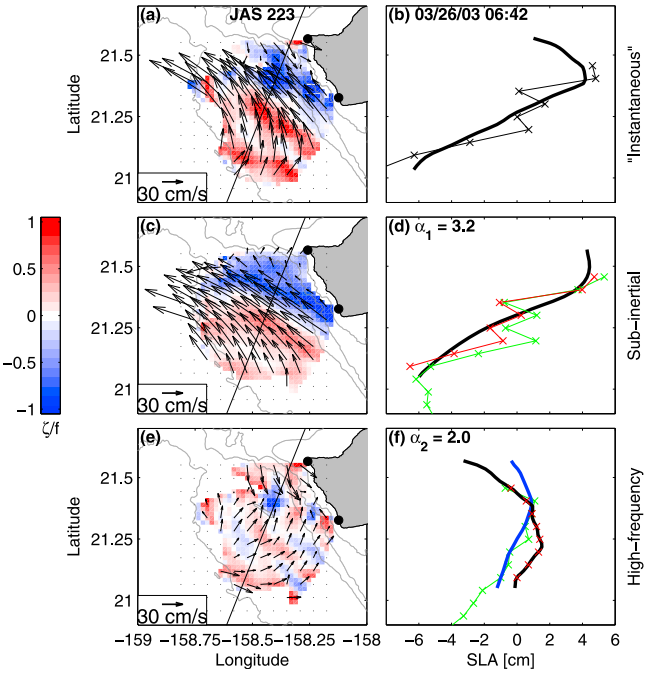

Figure 3. Same as Figure 2 but for Jason-1 223 ground track on 26 March 2003.

encompassing a broad band of increased energy near f in the clockwise current rotary spectrum (Figure 4a). To investigate the SLA contribution of the different high-frequency processes, we computed hourly time-series of the terms in the divergence equation from the HFR currents:

$$\frac{\partial \delta}{\partial t} + \nabla.(\mathbf{u}.\nabla\mathbf{u}) - f\zeta = -g\nabla^2 h \qquad (3)$$

with $\delta = \partial u/\partial x + \partial v/\partial y$ the divergence and $\zeta = \partial v/\partial x - \partial u/\partial y$ the relative vorticity. The effect on SLA, given by the r.h.s. of (3), is obtained by summing the terms on the l.h.s. The frequency spectra of each term of (3) are shown in Figure 4b. They reveal different regimes for different frequencies. For sub-inertial frequencies, the second and third terms dominate the first term on the l.h.s. of (3), consistent with gradient-wind balance. For near-inertial frequencies all three terms are important, although the second term is twice as large as the others. However, contrary to the clockwise kinetic energy which exhibits two peaks around f as large or larger than the diurnal tidal peaks (Figure 4a), the $\nabla^2 h$ spectrum is flat around f (while the diurnal peaks are detectable). This lack of NIO effect on SLA confirms recent numerical results [see *Klein et al.*, 2009, Figure 1c]. For super-inertial frequencies, the first term is preponderant and its energy is dominated by tides and their higher harmonics (Figure 4b).

[9] While barotropic tides are usually removed from altimeter observations using numerical predictions of the barotropic tides, baroclinic tides are not. Contribution from internal tides that remain phase-locked with astronomical forcing (thereafter coherent internal tides) can be extracted from altimeter observations by least-square fit (see below), using the aliased frequencies corresponding to tidal frequencies under-sampled at the relatively long repeat periods of satellite altimeters [*Ray and Mitchum*, 1996]. However, mesoscale currents are known to affect the propagation of internal tides [e.g., *Chavanne et al.*, 2010c], making them incoherent with astronomical forcing. The contribution from incoherent internal tides cannot be removed by least-square fit. It is thus important to compare the SLA contribution from super-inertial motions (which include incoherent internal tides), h'_{hfr} (thick black lines on Figures 2f and 3f), with that from coherent internal tides, $\hat{h}_{hfr}$ (thick blue lines), obtained by using (1) with the coherent tidal currents extracted by least-square fitting all the constituents shown in Figure 4 to the HFR currents over each 2-month period of uninterrupted coverage in Fall 2002 and Spring 2003. The contribution from incoherent internal tides, taken as $\tilde{h}_{hfr} = h'_{hfr} - \hat{h}_{hfr}$, is compared with the contribution from coherent internal tides, $\hat{h}_{hfr}$, using the ratio of their rms values along the altimeter tracks: $\alpha_2 = rms(\tilde{h}_{hfr})/rms(\hat{h}_{hfr})$. For the GFO pass over the anticyclone, the contribution from coherent internal tides was dominant ($\alpha_2 = 0.7 < 1$ (Figure 2f)), while for the Jason-1 pass over the VRW, the contribution from incoherent internal tides was dominant ($\alpha_2 = 2.0 > 1$). These two cases are representative of the 20 passes analyzed since α_2 ranges from 0.3 to 2.0, with 7 passes having $\alpha_2 \geq 1$, indicating a dominant incoherent internal tide contribution for these 7 passes.

[10] We now extract the coherent internal tide contribution from altimeter observations by least-square fit. SLA observations were available for 6.5 years (3 May 2002 to 17 October 2008) for Jason-1 and for 8.3 years (25 January 2000 to 17 May 2008) for GFO, long enough to separate the aliased tidal frequencies that were significant to 85% confidence level (determined by bootstrapping): (M_2, S_2,

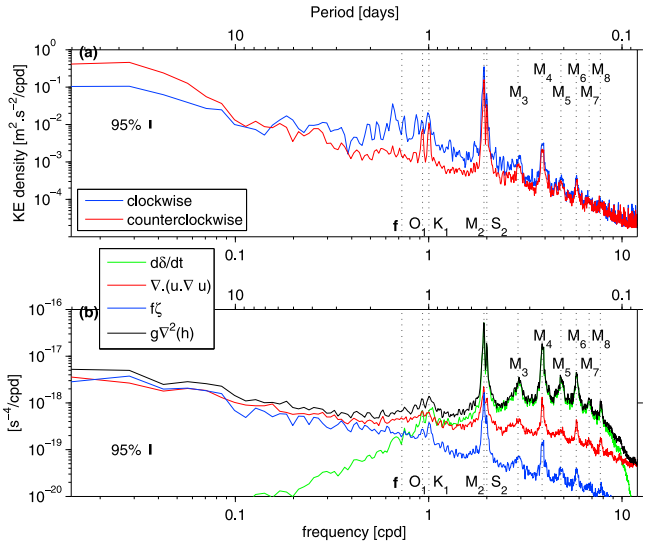

Figure 4. (a) Rotary spectra of HFR surface currents (blue: clockwise; red: counter-clockwise) computed over a 2-month period of almost uninterrupted coverage in Fall 2002. (b) Spectra of the terms in the divergence equation (3), as indicated in the legend. Spectra were averaged over grid points with more than 90% temporal coverage (missing observations were filled by linear interpolation). 95% confidence intervals assume that 1 out of 9 grid points are independent. Inertial f and tidal frequencies are indicated by vertical dotted lines.

M_3, M_4, M_5, M_6) for GFO-13 and (M_2, S_2, K_1, M_5, M_6) for JAS-223. The resulting coherent M_2 SLA contributions are shown in Figure 1. As first reported by *Ray and Mitchum* [1996], the oscillation along JAS-223, with a wavelength of ~150 km, is due to mode-1 internal M_2 tides propagating almost parallel to JAS-223 away from their generation location in the Kaua'i Channel. The coherent SLA contributions from all the tidal constituents extracted (green lines on Figures 2f and 3f) display domings with amplitudes similar to those obtained from the coherent tidal currents (blue lines). However, whether correcting the observed SLA for the contribution of coherent internal tides extracted from the altimeter observations (green lines on Figures 2d and 3d), or for the super-inertial contribution obtained from the HFRs (red lines), the random instrumental noise prevents computing accurate cross-track currents using gradient-wind or geostrophic balances (a conclusion corroborated by the 18 other passes).

4. Discussion

[11] The simultaneous availability of along-track SLA observations from two satellite altimeters and high-resolution 2-D surface current observations from HFRs deployed on the west shore of O'ahu, Hawai'i, made it possible to investigate whether submesoscale processes could be resolved by altimetry. Along-track SLAs were computed from the HFR observations by integrating the inviscid PE momentum equation along the satellite tracks, enabling an estimation of the relative contribution of high and low frequency motions to SLA. We focused on two case studies representative of the 20 cases analyzed. For the GFO pass over the anticyclonic vortex, SLA was dominated by the high-frequency contribution, while the low-frequency contribution dominated SLA for the Jason-1 pass over the VRW. The high-frequency contribution mostly involves tidal motions that include diurnal and semi-diurnal frequencies as well as their higher harmonics. Near-inertial motions on the other hand do not appear to have any impact on the SLA, as suggested by *Klein et al.* [2009].

[12] When the contribution of tidal motions is removed from the SLA observed by conventional altimetry the residual SLA is, not surprisingly, much too noisy to capture the submesoscale structures (Figures 2d and 3d). Planned future satellite missions such as Surface Water and Ocean Topography (SWOT) [*Fu and Ferrari*, 2008], with its targeted noise level of 1 cm of random error at a sampling rate of 1 km, may enable us to resolve submesoscale processes with scales $\mathcal{O}$ (10 km), once the internal tide contributions are removed. The contribution of coherent internal tides can be removed from long altimeter missions by using a least-square fit technique [*Ray and Mitchum*, 1996], but the main result of the present study is that this is not always sufficient: contribution of incoherent internal tides can be large, as revealed in the VRW case (representative of 7 of the 20 passes analyzed). Thus, to correct SLA observations for the total contribution from internal tides, it will be necessary to predict accurately the ocean mesoscale variability, in order to take into account its effect on internal tide propagation [*Arbic et al.*, 2010] and therefore the contribution of the incoherent internal tides.

[13] **Acknowledgments.** Along-track altimeter data were produced by Ssalto/Duacs and distributed by Aviso (http://www.aviso.oceanobs.com/). The HFRs and their deployment were funded by the National Science Foundation; full acknowledgments are given by *Chavanne et al.* [2010d]. We thank both reviewers and the editor who contributed to improve the manuscript.

References

Arbic, B. K., A. J. Wallcraft, and E. J. Metzger (2010), Concurrent simulation of the eddying general circulation and tides in a global ocean model, *Ocean Modell.*, *32*, 175–187.

Capet, X., J. C. McWilliams, M. J. Molemaker, and A. F. Shchepetkin (2008), Mesoscale to submesoscale transition in the California Current system. Part I: Flow structure, eddy flux, and observational tests, *J. Phys. Oceanogr.*, *38*, 29–43.

Chavanne, C., P. Flament, and K.-W. Gurgel (2010a), Interactions between a submesoscale anticyclonic vortex and a front, *J. Phys. Oceanogr.*, *40*, 1802–1818.

Chavanne, C., P. Flament, D. Luther, and K.-W. Gurgel (2010b), Observations of vortex rossby waves associated with a mesoscale cyclone, *J. Phys. Oceanogr.*, *40*, 2333–2340.

Chavanne, C., P. Flament, D. Luther, and K.-W. Gurgel (2010c), The surface expression of semi-diurnal internal tides near a strong source at Hawai'i. Part II: Interactions with mesoscale currents, *J. Phys. Oceanogr.*, *40*, 1180–1200.

Chavanne, C., P. Flament, E. Zaron, G. Carter, M. Merrifield, D. Luther, and K.-W. Gurgel (2010d), The surface expression of semi-diurnal internal tides near a strong source at Hawai'i. Part I: Observations and numerical predictions, *J. Phys. Oceanogr.*, *40*, 1155–1179.

Chelton, D. B., M. G. Schlax, R. M. Samelson, and R. A. de Szoeke (2007), Global observations of large oceanic eddies, *Geophys. Res. Lett.*, *34*, L15606, doi:10.1029/2007GL030812.

Ducet, N., P. Le Traon, and G. Reverdin (2000), Global high-resolution mapping of ocean circulation from TOPEX/Poseidon and ERS-1 and -2, *J. Geophys. Res.*, *105*(C8), 19,477–19,498.

Fu, L. L., and R. Ferrari (2008), Observing oceanic submesoscale processes from space, *Eos Trans. AGU*, *89*(48), doi:10.1029/2008EO480003.

Klein, P., G. Lapeyre, and W. G. Large (2004), Wind ringing of the ocean in presence of mesoscale eddies, *Geophys. Res. Lett.*, *31*, L15306, doi:10.1029/2004GL020274.

Klein, P., B. L. Hua, G. Lapeyre, X. Capet, S. Le Gentil, and H. Sasaki (2008), Upper ocean turbulence from high-resolution 3-D simulations, *J. Phys. Oceanogr.*, *38*, 1748–1763.

Klein, P., J. Isern-Fontanet, G. Lapeyre, G. Roullet, E. Danioux, B. Chapron, S. Le Gentil, and H. Sasaki (2009), Diagnosis of vertical velocities in the upper ocean from high resolution sea surface height, *Geophys. Res. Lett.*, *36*, L12603, doi:10.1029/2009GL038359.

Ray, R. D., and G. T. Mitchum (1996), Surface manifestation of internal tides generated near Hawaii, *Geophys. Res. Lett.*, *23*(16), 2101–2104.

C. P. Chavanne, School of Environmental Sciences, University of East Anglia, Norwich, NR4 7TJ, UK. (cedric.chavanne@ensta.org)

P. Klein, Laboratoire de Physique des Océans, IFREMER-CNRS-UBO-IRD, BP 70, F-29280 Plouzane CEDEX, France.